NASA/CR—2001-211072

Solar Collector With Image-Forming Mirror Cavity to Irradiate Small Central Volume

Don Buchele and Charles Castle
Northland Scientific Inc., Olmsted Falls, Ohio

Joseph A. Bonometti
University of Alabama, Huntsville, Huntsville, Alabama

September 2001

The NASA STI Program Office . . . in Profile

Since its founding, NASA has been dedicated to the advancement of aeronautics and space science. The NASA Scientific and Technical Information (STI) Program Office plays a key part in helping NASA maintain this important role.

The NASA STI Program Office is operated by Langley Research Center, the Lead Center for NASA's scientific and technical information. The NASA STI Program Office provides access to the NASA STI Database, the largest collection of aeronautical and space science STI in the world. The Program Office is also NASA's institutional mechanism for disseminating the results of its research and development activities. These results are published by NASA in the NASA STI Report Series, which includes the following report types:

- TECHNICAL PUBLICATION. Reports of completed research or a major significant phase of research that present the results of NASA programs and include extensive data or theoretical analysis. Includes compilations of significant scientific and technical data and information deemed to be of continuing reference value. NASA's counterpart of peer-reviewed formal professional papers but has less stringent limitations on manuscript length and extent of graphic presentations.

- TECHNICAL MEMORANDUM. Scientific and technical findings that are preliminary or of specialized interest, e.g., quick release reports, working papers, and bibliographies that contain minimal annotation. Does not contain extensive analysis.

- CONTRACTOR REPORT. Scientific and technical findings by NASA-sponsored contractors and grantees.

- CONFERENCE PUBLICATION. Collected papers from scientific and technical conferences, symposia, seminars, or other meetings sponsored or cosponsored by NASA.

- SPECIAL PUBLICATION. Scientific, technical, or historical information from NASA programs, projects, and missions, often concerned with subjects having substantial public interest.

- TECHNICAL TRANSLATION. English-language translations of foreign scientific and technical material pertinent to NASA's mission.

Specialized services that complement the STI Program Office's diverse offerings include creating custom thesauri, building customized data bases, organizing and publishing research results . . . even providing videos.

For more information about the NASA STI Program Office, see the following:

- Access the NASA STI Program Home Page at ***http://www.sti.nasa.gov***

- E-mail your question via the Internet to help@sti.nasa.gov

- Fax your question to the NASA Access Help Desk at 301–621–0134

- Telephone the NASA Access Help Desk at 301–621–0390

- Write to:
  NASA Access Help Desk
  NASA Center for AeroSpace Information
  7121 Standard Drive
  Hanover, MD 21076

NASA/CR—2001-211072

Solar Collector With Image-Forming Mirror Cavity to Irradiate Small Central Volume

Don Buchele and Charles Castle
Northland Scientific Inc., Olmsted Falls, Ohio

Joseph A. Bonometti
University of Alabama, Huntsville, Huntsville, Alabama

Prepared under Marshall Space Flight Center Grant C–71734–K

National Aeronautics and
Space Administration

Glenn Research Center

September 2001

Contents were reproduced from the best available copy
as provided by the authors.

Available from

NASA Center for Aerospace Information
7121 Standard Drive
Hanover, MD 21076

National Technical Information Service
5285 Port Royal Road
Springfield, VA 22100

Available electronically at http://gltrs.grc.nasa.gov/GLTRS

Solar Collector with Image-Forming Mirror Cavity

to Irradiate Small Central Volume

Table of Contents

Background 1

Introduction 1

Design and Analysis 3

- IMAGE VOLUME IRRADIATED 3
- TARGET SELECTION 5
- FLAT TARGET FLUX LOSS 6
- BEAM BLOCKING BY PROBE 11
- FLAT TARGET IMAGE BLUR WITH HEMISPHERE 11
- FLAT TARGET IMAGE BLUR WITH ELLIPSOID 15
- TEMPERATURE OF FLAT TARGET WITH NO INFRARED REFLECTION LENS COAT 18
  - *Power Absorbed by Target* 18
  - *Thermal Power Radiated From Target* 19
- INCREASED POWER ON FLAT TARGET OF GIVEN TEMPERATURE 20
  - *With Infrared Reflection Coat on Lens* 20
- ALIGNMENT OF TARGET IN CAVITY 21
- ELLIPSE EQUATIONS 21

Concluding Remarks 21

Appendix I. Power into Target 27

Appendix II. Thermal Power Radiation From Target 27

- HEMISPHERE 28
- ELLIPSOID 28

Reference 29

Solar Collector with Image-Forming Mirror Cavity to Irradiate Small Central Volume

BACKGROUND

The NASA Glenn Research Center and the University of Alabama, Huntsville (UAH), Dept. of Physics has been actively involved in research areas dealing with the concentration of solar energy and the generation of high temperature plasma research. While working on Marshall Space Flight Center's "Shooting Star" project, personnel at UAH, the NASA Glenn Research Center (GRC) and Northland Scientific Inc. (NSI) were engaged in the design and test of a unique refractive secondary solar concentrator for the "Shooting Star" thermal propulsion engine. As a result of this collaboration the idea evolved that a similar secondary solar concentrator might be used to generate temperatures high enough to either create or sustain a plasma which in turn could be used to heat a gaseous propellant to produce thrust. It was decided at that time that NSI optics personnel would evaluate how a new design secondary concentrator might be used in conjunction with the UAH Solar Lab's primary concentrator to produce solar flux concentrations high enough to evaluate and/or demonstrate the concept. It was further believed that such a device could also be utilized for high temperature materials research since specimens could be heated to ultra high temperatures.

Various secondary concentrator optical designs and configurations were considered by NSI that would produce the maximum concentration of solar energy. The design that was selected was one that would not only maximize solar concentration but would minimize infra red heat loss from the high temperature plasma or heated material specimen. The following report is intended to provide the researcher with all the information needed to fully understand the underlining theory and proper operation of the hardware provided.

INTRODUCTION

The UAH Solar Laboratory collector of ten-foot diameter, nine-foot focal length in Fig.1(a) focuses a 2-inch diameter sun image containing five kilowatts. Preceding this focal plane, a lens in Fig. 1(b) focuses a smaller sun image 1.37 inches diameter at the inlet hole of a mirror cavity. An important task of the lens is to focus two image planes at prescribed positions, the sun at the cavity entrance, and the collector at the junction of the ellipsoid and hemisphere cavity surfaces. The right half of the cavity is an ellipsoid reflector that focuses a smaller final image of the 1.37-inch sun image. The beam converges within a hemisphere solid angle to the image. The image is 2.8 inches away from the nearest cavity surface to minimize mirror dirtying by a heated target placed at the image. To the left of the ellipsoid a hemisphere mirror has its center of curvature at the image. Any rays

going from the target to the hemisphere mirror are reflected back to it to reduce radiated power loss.

Reference 1 describes nonimaging optical concentrators for a solar primary collector. These applications do not heat a target to incandescence, or place the target at a distance from the optical surfaces that are held to ambient temperature. To reach a high target temperature, its thermal radiation power loss must be minimized. These requirements led to the present design of an image forming optical system.

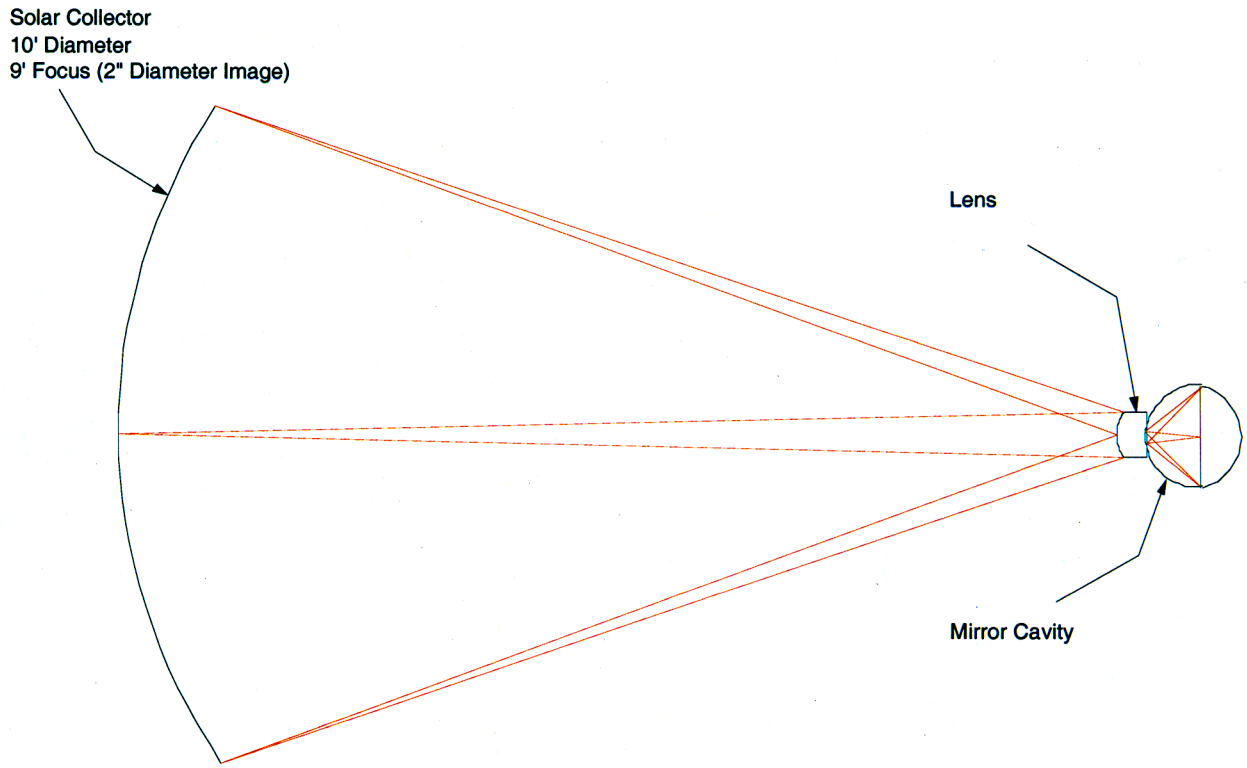

Figure 1(a) Solar Collector with Mirror Cavity, Overall Ray Path

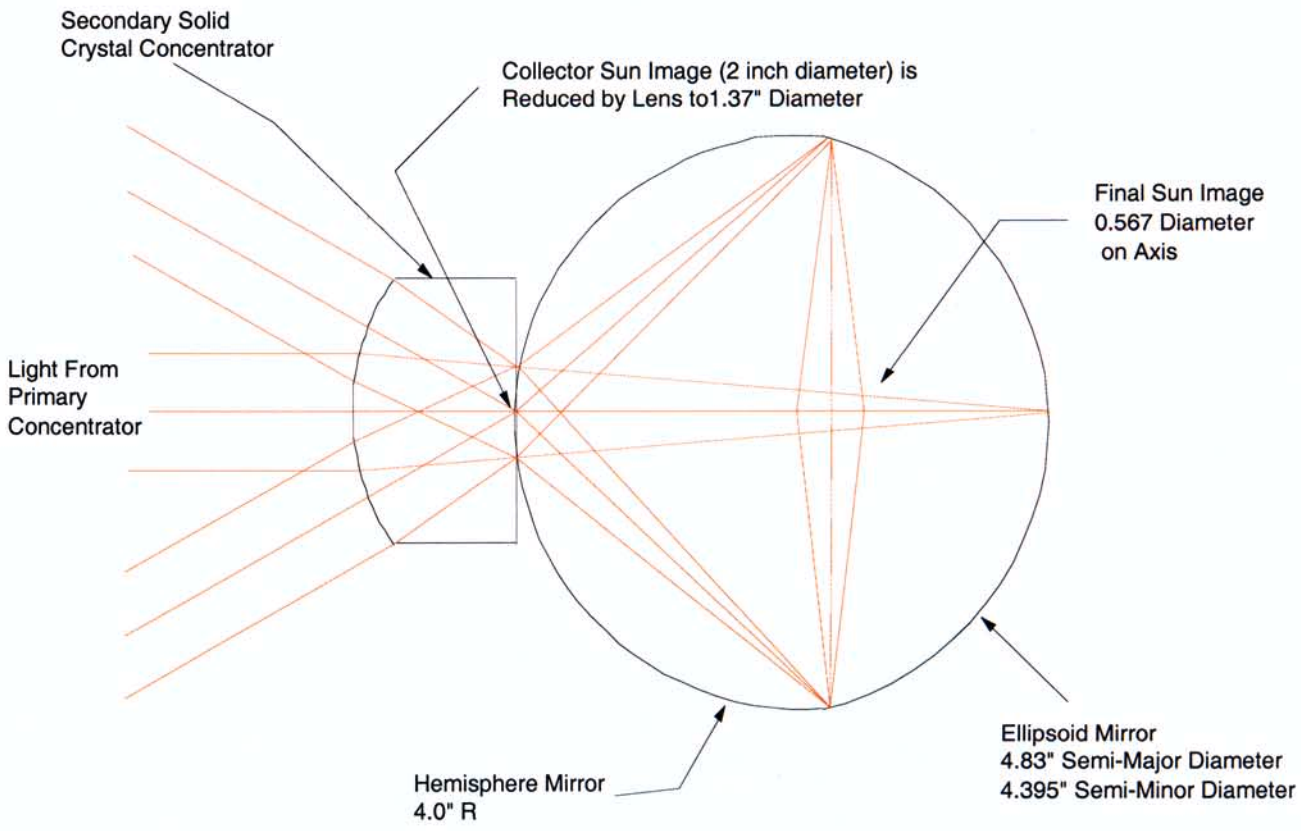

Figure 1(b) Ray Path in Cavity with Lens Focal Planes

For an ideal collector of nine-foot focal length, the sun image subtends 0.53 degrees, giving an image diameter of 1.0-inch. Collector aberration gives a maximum irradiance on axis and a smaller value at the 2-inch diameter. This aberrated distribution is preserved by the image-forming lens and cavity of Fig.1. The lens and cavity re-image this distribution at the final image. The report calculations use an average uniform distribution.

DESIGN AND ANALYSIS

IMAGE VOLUME IRRADIATED

A ray trace in Fig.2 has two focal points on opposite edges of the 1.37-inch sun image at the lens surface. A ray from each point on the sun image to one point on the ellipsoid is the cross-section of a cone containing all rays from the sun image to that point on the ellipsoid. After reflection from the ellipsoid the cone cross-section at the target

is an illuminated elliptical area. The target volume has cross-sections shown in the table for three incident angles θ of 0, 45 and 90 degrees. The sections can all contain a spherical volume 0.567-inch diameter that receives rays from the ellipsoid over a hemisphere solid angle 2π steradians. The larger beam cross-section at angles greater than zero degrees provides a tolerance for axial position of the target. A tolerance for transverse position is provided by a smaller target such as 0.5 inches used for examples in this report.

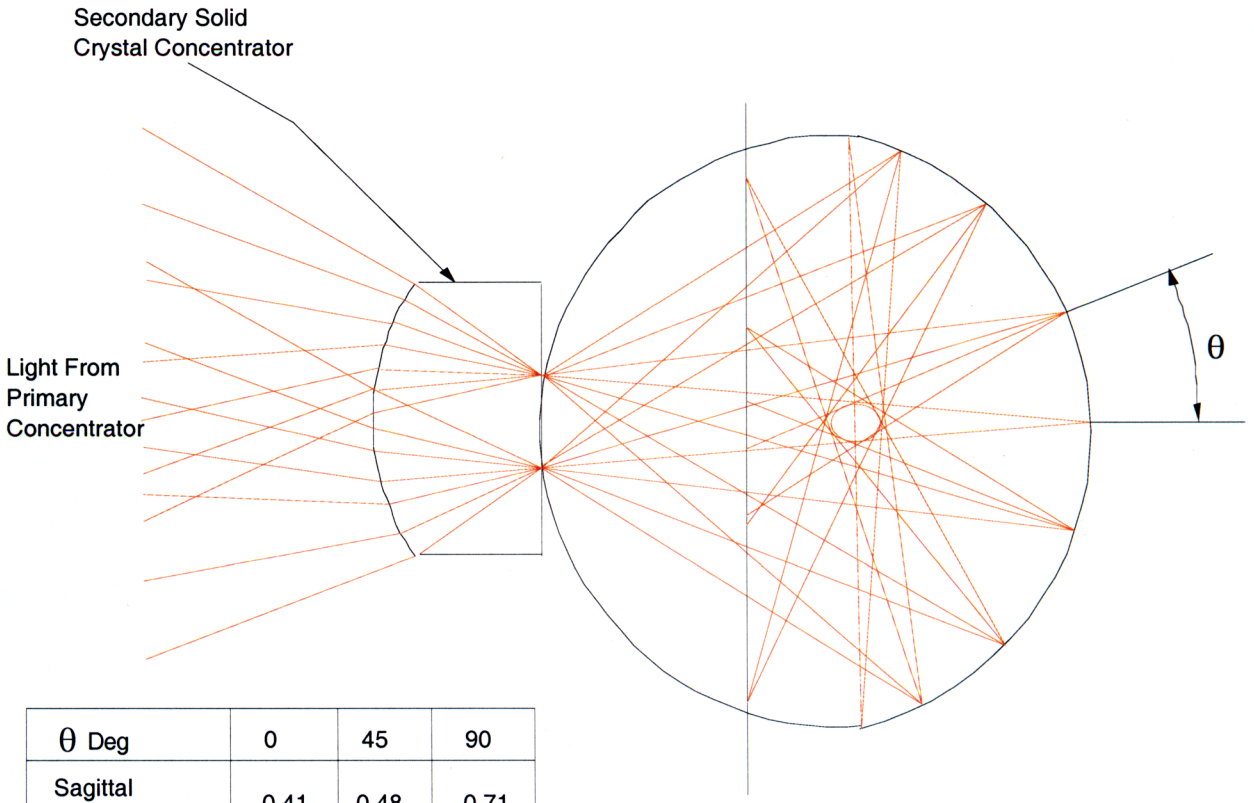

θ Deg	0	45	90
Sagittal Magnification	0.41	0.48	0.71
Target Cross-Section Diameters	0.567 (0.567)	0.658 (0.619)	0.968 (0.684)

Figure 2 Image Cross Sections to Define Irradiated Volume

Flux reflected or emitted from the target to the ellipsoid is focused at the lens. The lens may be coated to reflect some flux back to the ellipsoid and the target for a flux loss reduction as shown in Fig.3. For maximum efficiency the lens surface is concave. A ray path from the edge of the ellipsoid to the lens is reflected and focused to the opposite edge.

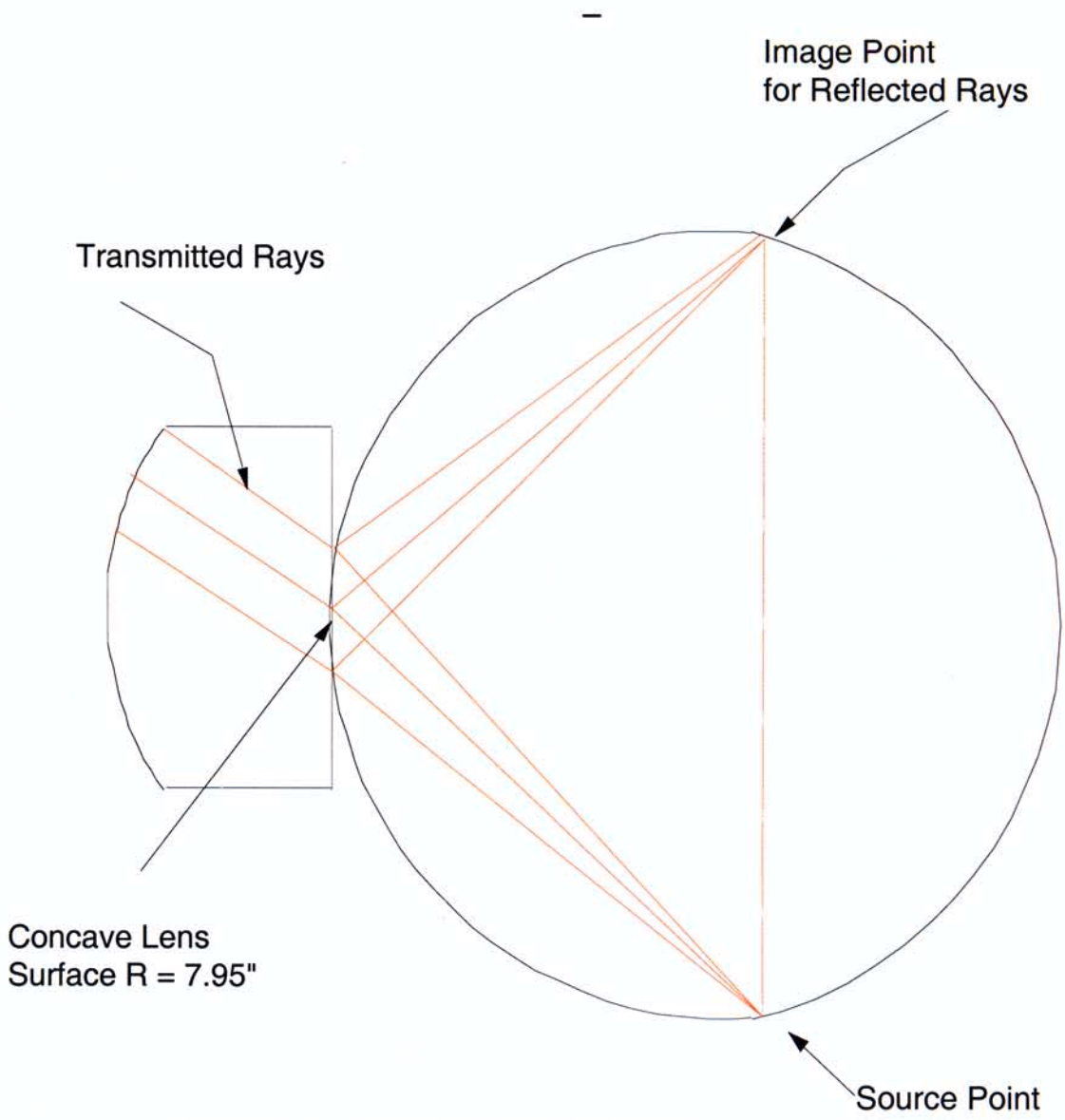

Figure 3 Concave Lens Surface

TARGET SELECTION

The cavity was designed for maximum irradiance on a spherical volume in a gas. The performance analysis is derived for a flat opaque plate 0.5-inch diameter as the first application of the cavity.

If the target is semi-transparent, solar rays that it transmits are reflected back by the hemisphere mirror, giving a subtended solid angle 4π steradian of incident flux. Within the 0.567-inch diameter sphere the flux density is a maximum. At larger diameters up to 0.968 inch, the

solid angle subtense and flux input is smaller. Reference 2 compares imaging and non-imaging systems to produce irradiance levels equal to the sun surface. The non-imaging system irradiates over a hemisphere solid angle with high efficiency. The image forming system in Fig. 2(a) irradiates a semi-transparent spherical volume over a spherical sold angle at reduced efficiency because some rays are outside the volume. Thus the irradiance level in the volume is ideally twice that at the sun surface.

If an opaque sphere such as a plasma is the target, the solar rays are incident over 2π steradians. The sphere can radiate over 2π steradians to the hemisphere mirror that reflects the rays back to the sphere. This reduces the flux loss by thermal radiation.

If an opaque flat surface is placed at the image, the solar rays are incident over 2π steradians, but the projected flat surface area goes to zero in the direction of its own plane. This reduces the intercepted solar flux by 0.5, and the other half missing the target is reflected back to the lens. The lens transmits part of the flux to the collector as a loss. The lens also reflects the other part of this flux to the ellipsoid and to a focus where it started next to the target. This flux misses the target and is also a loss.

Smoothness of the flat surface has no significant effect because the optics subtend a hemisphere on both sides of the surface. The edge of a flat surface receives flux from π steradians, half as much as the flat surface.

FLAT TARGET FLUX LOSS

Analysis uses the ray paths in Fig. 4 to define the reflection and transmission symbol subscripts used in the equations. Before reaching the target, the incident power ray path in Fig. 4(a) shows transmission loss τ at the two lens surfaces which include reflection by a coat on lens surface 2 , absorption loss by the quartz lens, and reflection loss by the ellipsoid mirror coat. The uncoated lens surfaces have a transmission factor 0.97. The quartz lens has a spectral transmission factor plotted in Fig.5. The solar spectrum at air mass 1.5 in Fig.6 includes the air absorption over a path length 1.5 the vertical path. The spectrum has very little flux past 2.4 micron where the quartz absorption begins, so the transmission factor in quartz is 1.0. The ellipsoid mirror coat of protected silver has an average reflectance of 0.96. The target also intercepts and absorbs flux directly from the lens that would otherwise go to the ellipsoid, so it is not a loss.

Flux reflected or emitted from the target is reflected and focused back to it by two paths in Fig. 4(a): to the hemisphere; and to the ellipsoid, lens, ellipsoid. This returned flux is necessary to produce a high target temperature. The returned flux is reduced by: 1) Reflection factor of the mirror and lens surfaces. 2) Beam blocking by probes for the target and measuring instruments. 3) Target image blur causes some

focused rays to miss the target at its edge. 4) Position error of the target that causes its image to be shifted from the target edge. Near the center of the spherical volume, a further increase of irradiance is produced because the cavity re-images the peaked irradiance distribution at the collector focus. This irradiance at the volume center is less affected by cavity surface fabrication error that causes image blur.

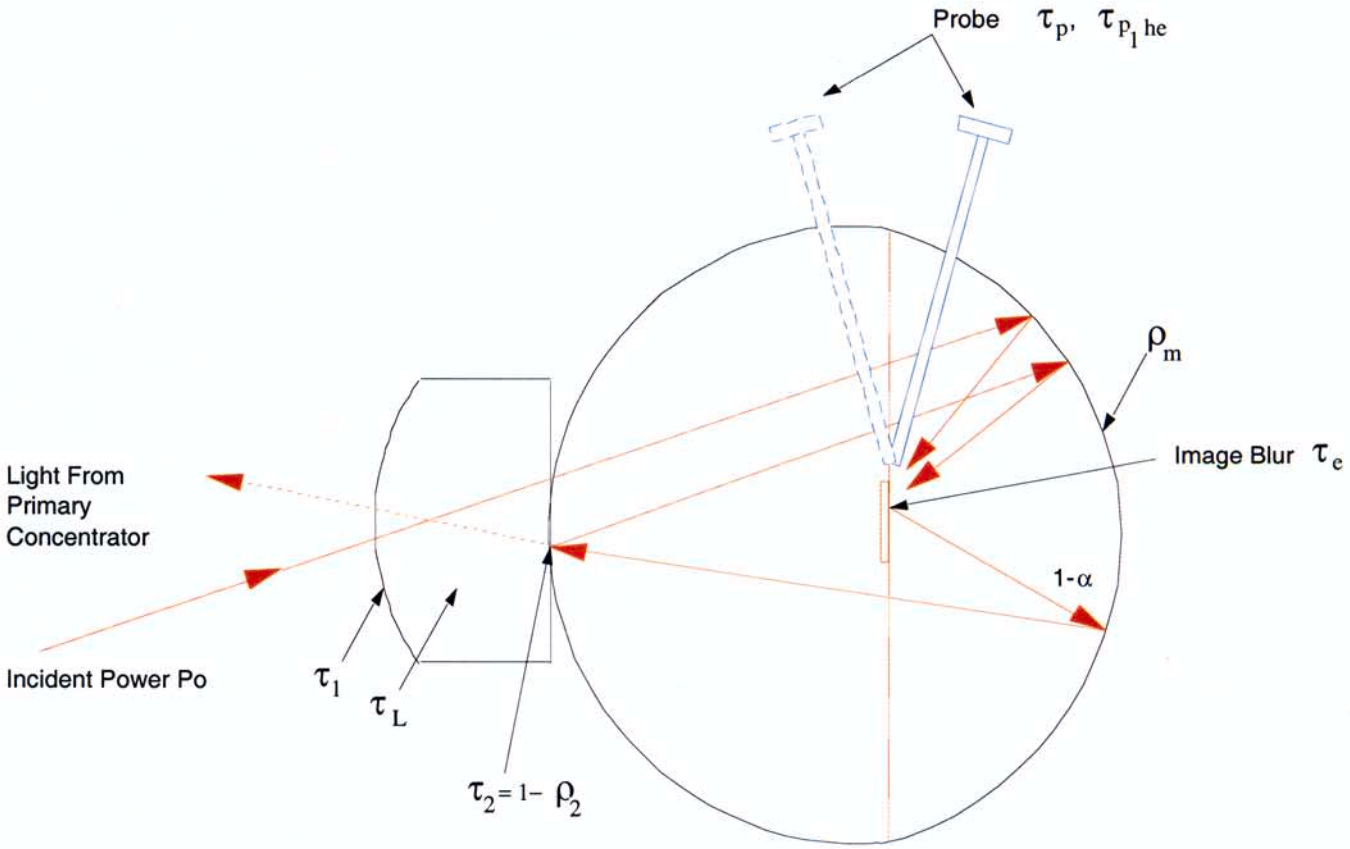

Figure 4(a) Ray Paths In Cavity; Solar Input and Reflection

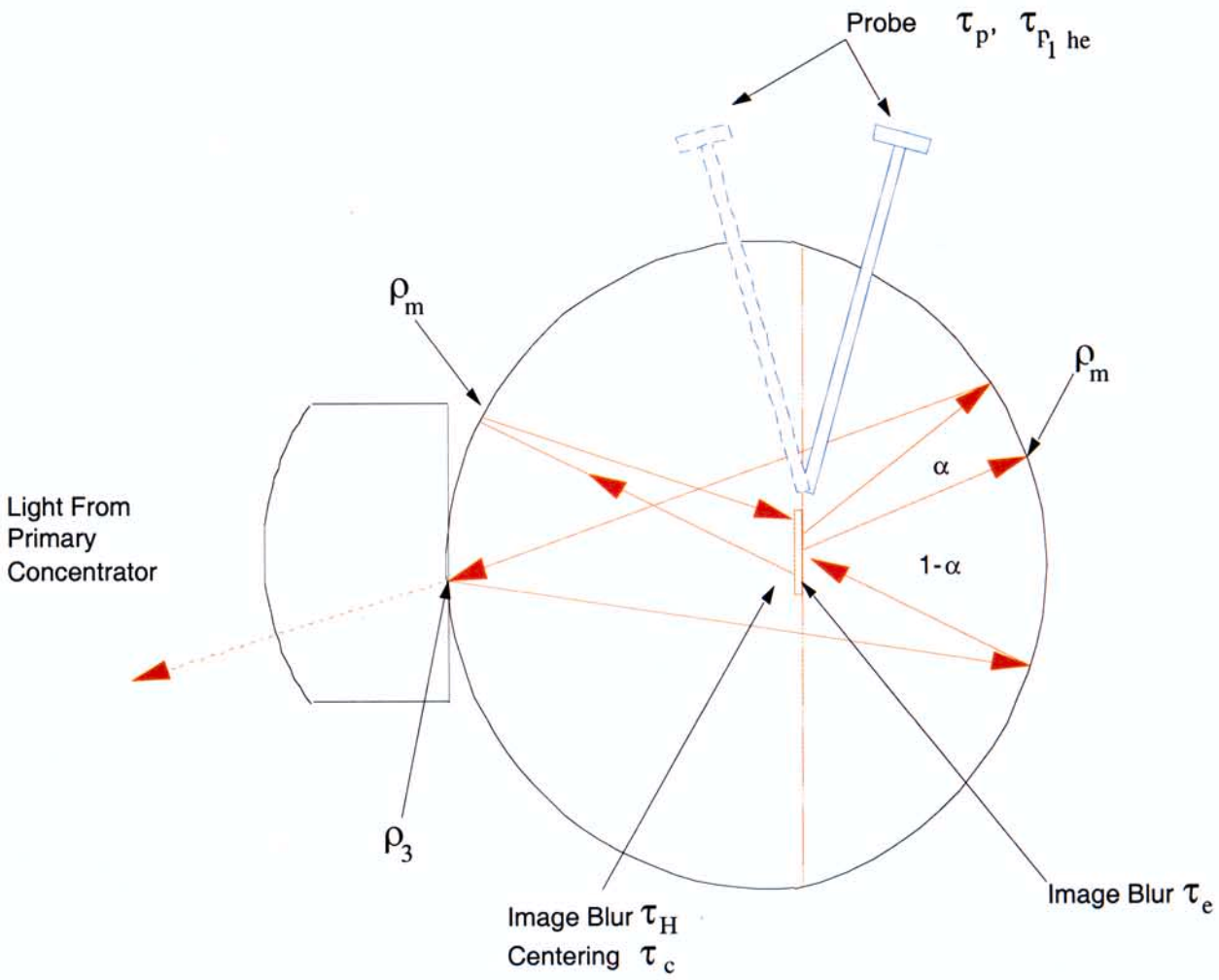

Figure 4(b) Ray Paths In Cavity; Target Radiation and Reflection

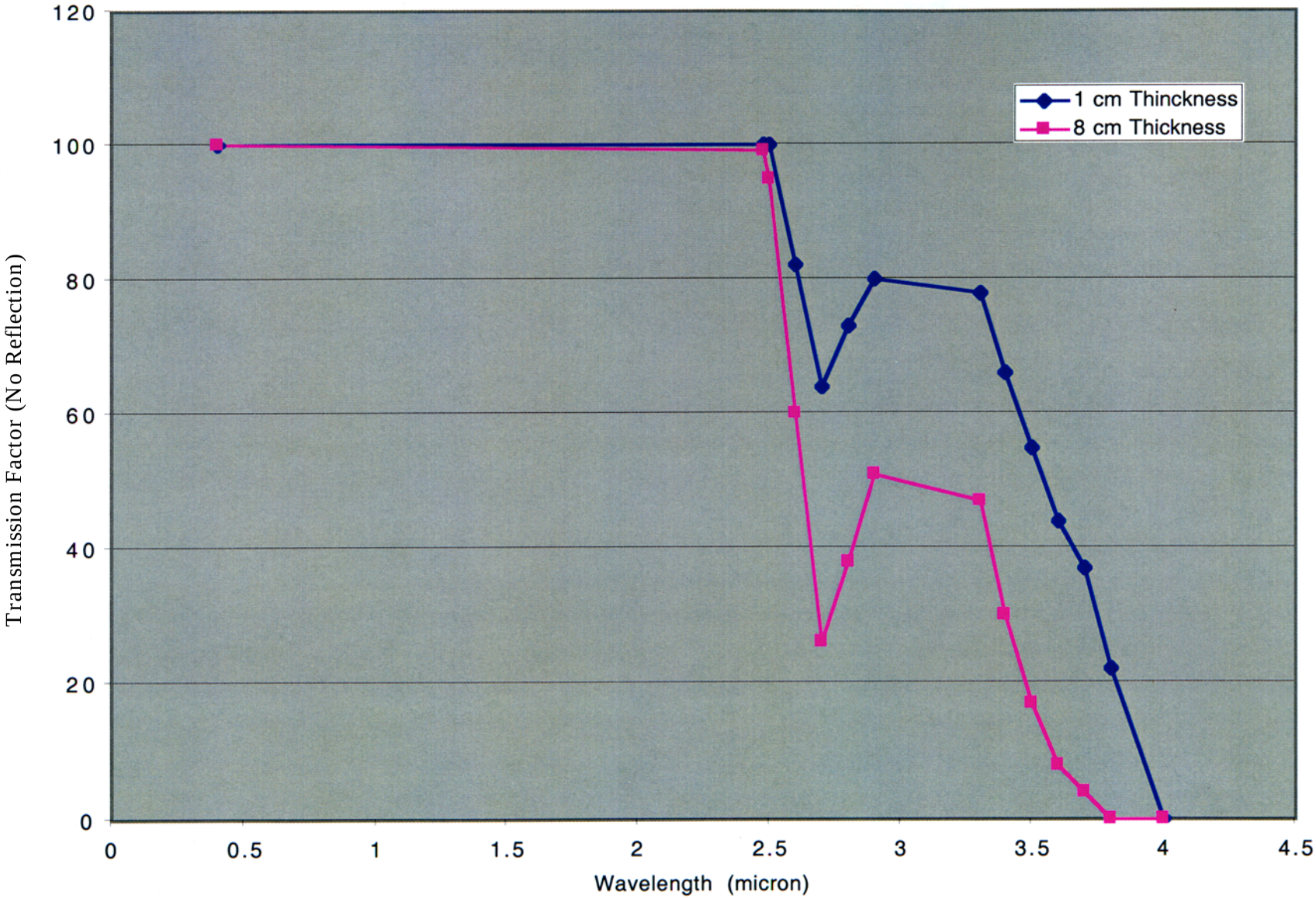

Figure 5 Transmission Factor of Number 124 Fused Quartz

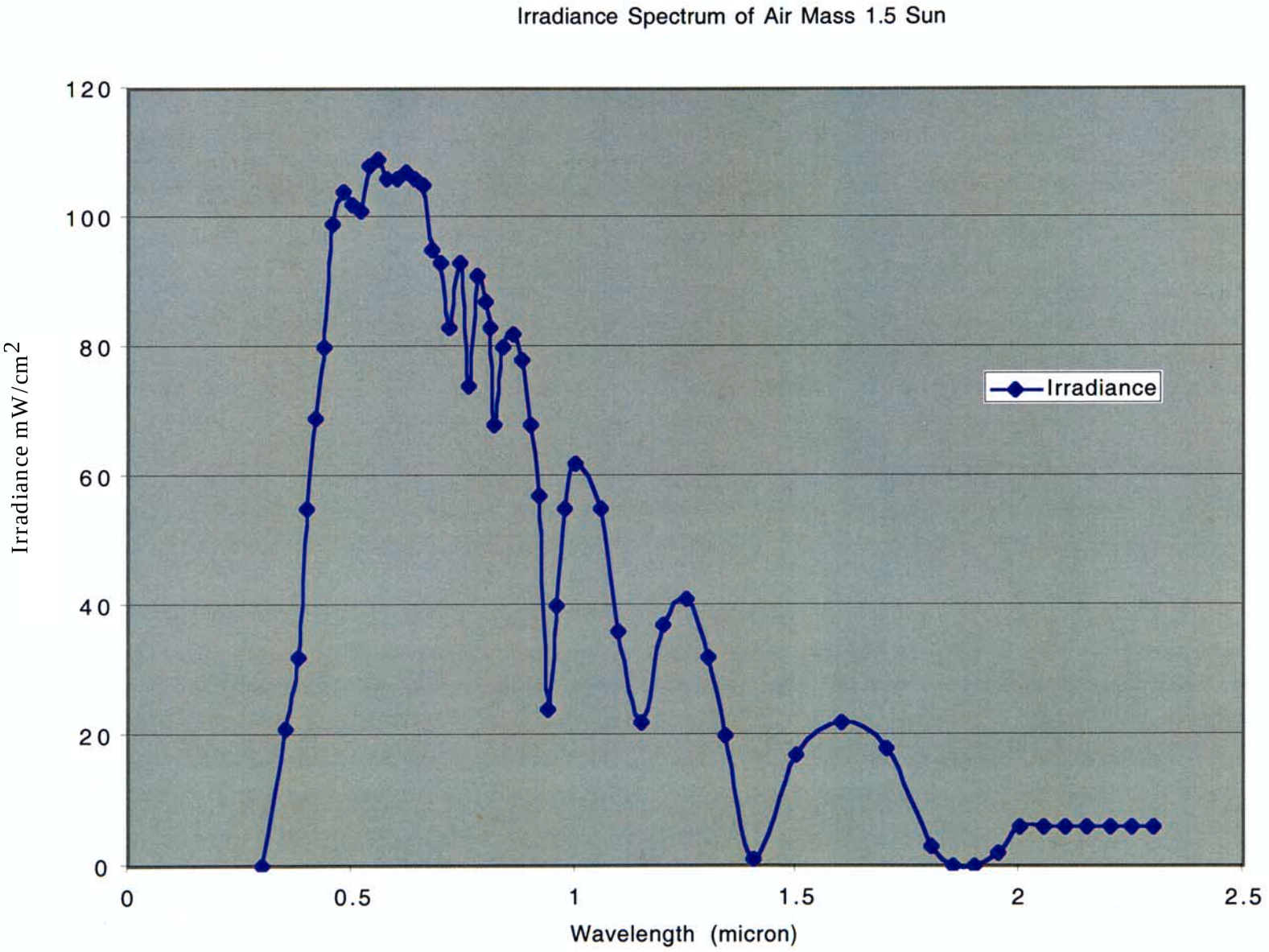

Figure 6 Irradiance Spectrum of Air Mass 1.5 Sun

BEAM BLOCKING BY PROBE

The target may be supported by a probe, in figure 4(b), from the cavity wall near the plane of the hemisphere and ellipsoid edges. The probe intercepts a fraction of the beam area for the beam going between the ellipsoid and the lens surface. A probe .25 inch diameter, 3.5 inches long has an area 0.02 of the 8-inch diameter beam area. This is a transmission factor $\tau_{P,HE}$ =0.98 for one pass. The probe also intercepts the beam converging to the target from the hemisphere or from the ellipsoid, giving τ_P. This blocks the beam in a solid angle that is a fraction of the hemispherical solid angle 2π steradian. The total interception depends on the distance of each probe segment from the target. The transmission factors are approximately 0.99 for a probe subtending 25 degrees in the azimuth and radial directions.

FLAT TARGET IMAGE BLUR WITH HEMISPHERE

A flat target and its image formed by the hemisphere are shown by the ray trace in Fig. 7(a). A point source at the edge of a 0.5 inch diameter target is focused at the opposite edge as shown in detail by the enlarged view. An important condition is that the object and image are always on the same target plane that can move axially relative to the mirror. For the image point to fall on the target edge, the target must be circular or a polygon with an even number of sides for symmetry. The best focus of the target edge has the target 0.002 inches from the center of the hemisphere.

The target must be accurately centered, since transverse displacement causes its image on the target to move in the opposite direction. This causes a flux loss that can set a position tolerance. For example, a target shift of 0.01 inch moves the image 0.02 inches from the target edge. This is a fractional flux loss 0.02/0.5 or four percent giving a transmission factor τ_C = .96.

The ray trace display of the blur diagram in this example includes rays that fill the hemisphere except for the area within 6 degrees from its edge. This angle contains one percent of the flux from a flat surface. The rays for flux calculation are distributed over the hemisphere aperture by the Zemax program as a tangent function that has fewer rays near the aperture edge. This corrects for the large angle of incidence on a flat target that reduces its projected area and makes each ray represent the same fraction of total flux.

The flux lost by image blur at the target edge is measured by integration vertically across the blur spot in Fig. 7(a). The Zemax graph of edge response in Fig. 7(b,c) is an integral over the blur spot from R=0 to R. The cross-hatched area under the curve at a radius greater than 0.25 is the flux loss. This area is measured and set equal to the rectangle with amplitude 1.0 and width ΔR. The width ΔR is an annulus inside the circular target representing flux loss. Then the flux

loss gives a transmission factor for the hemisphere with image blur

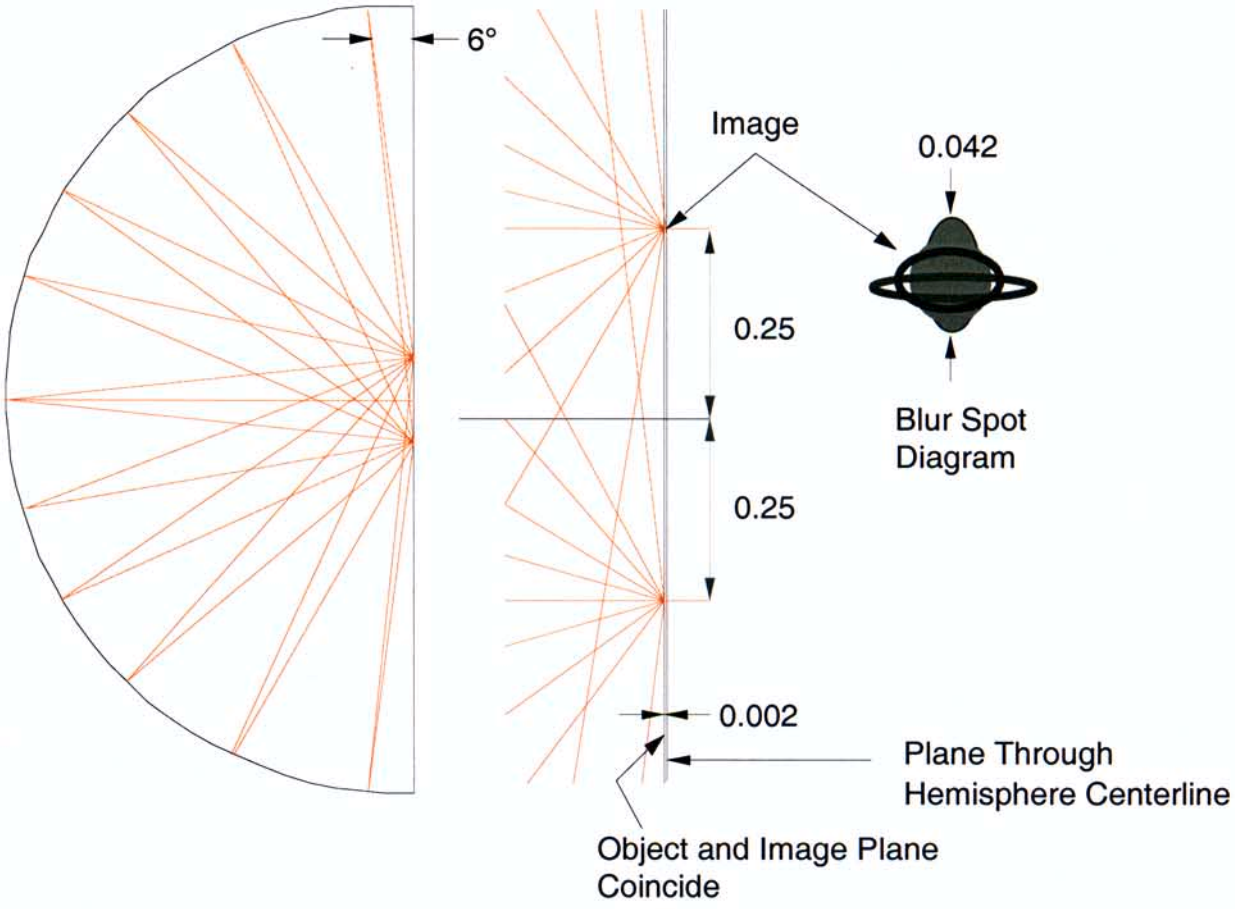

Figure 7(a) Hemisphere Image Blur; Ray Trace

$$\tau_H = (R-\Delta R)^2/R^2 \qquad (1)$$

The edge response curve and τ_H change with axial position of the target plane (this is plotted in figure (7c)). The maximum, 0.97, is at a distance 0.002 inches, which is also the hemisphere centerline position. An axial shift of -0.005 inch reduces the transmission factor from 0.97 to 0.92, a reduction of five percent. This graph is useful for choosing an axial position tolerance that depends on the importance of the transmission factor.

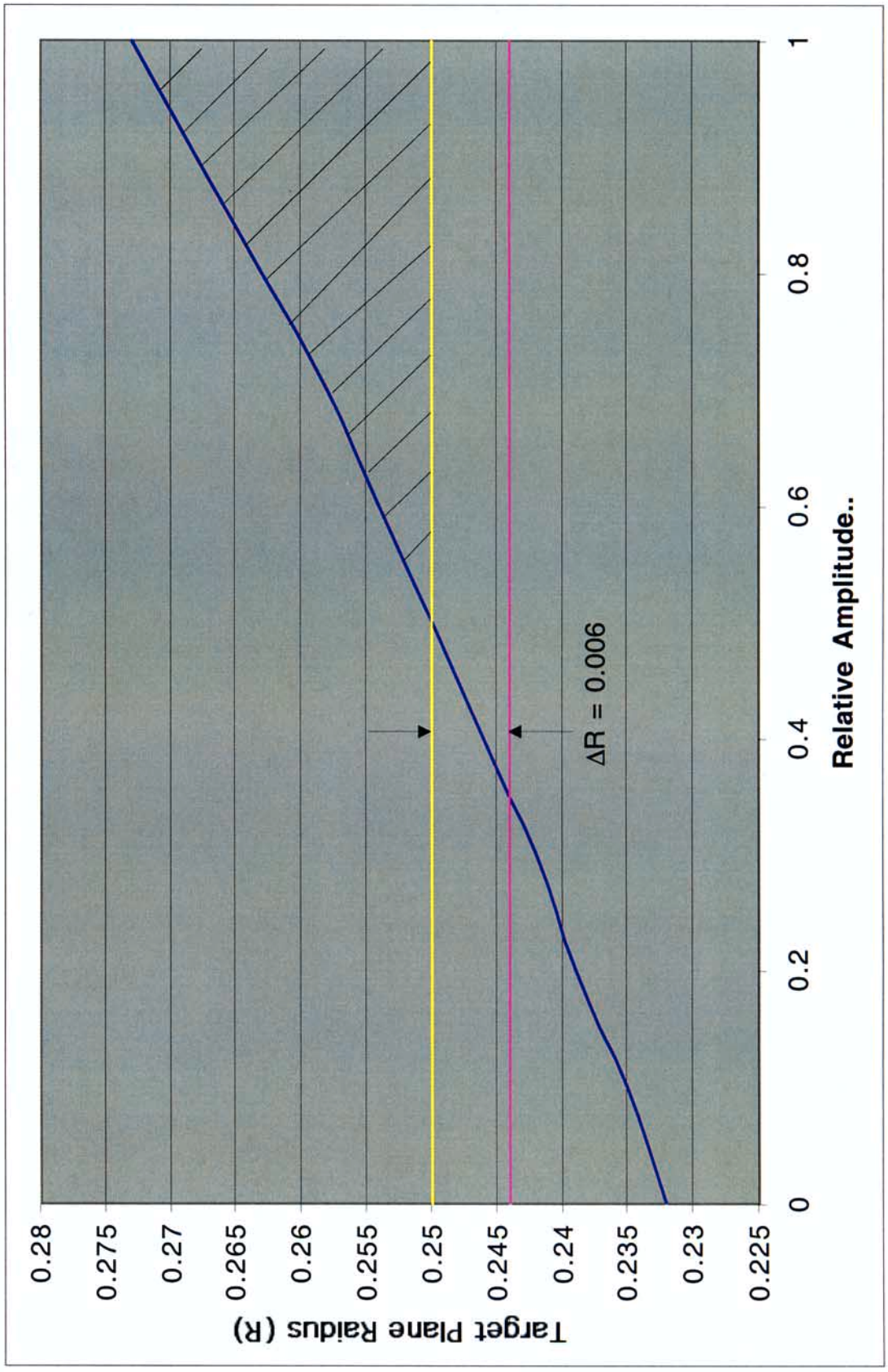

Figure 7(b) Edge Response of Point Image

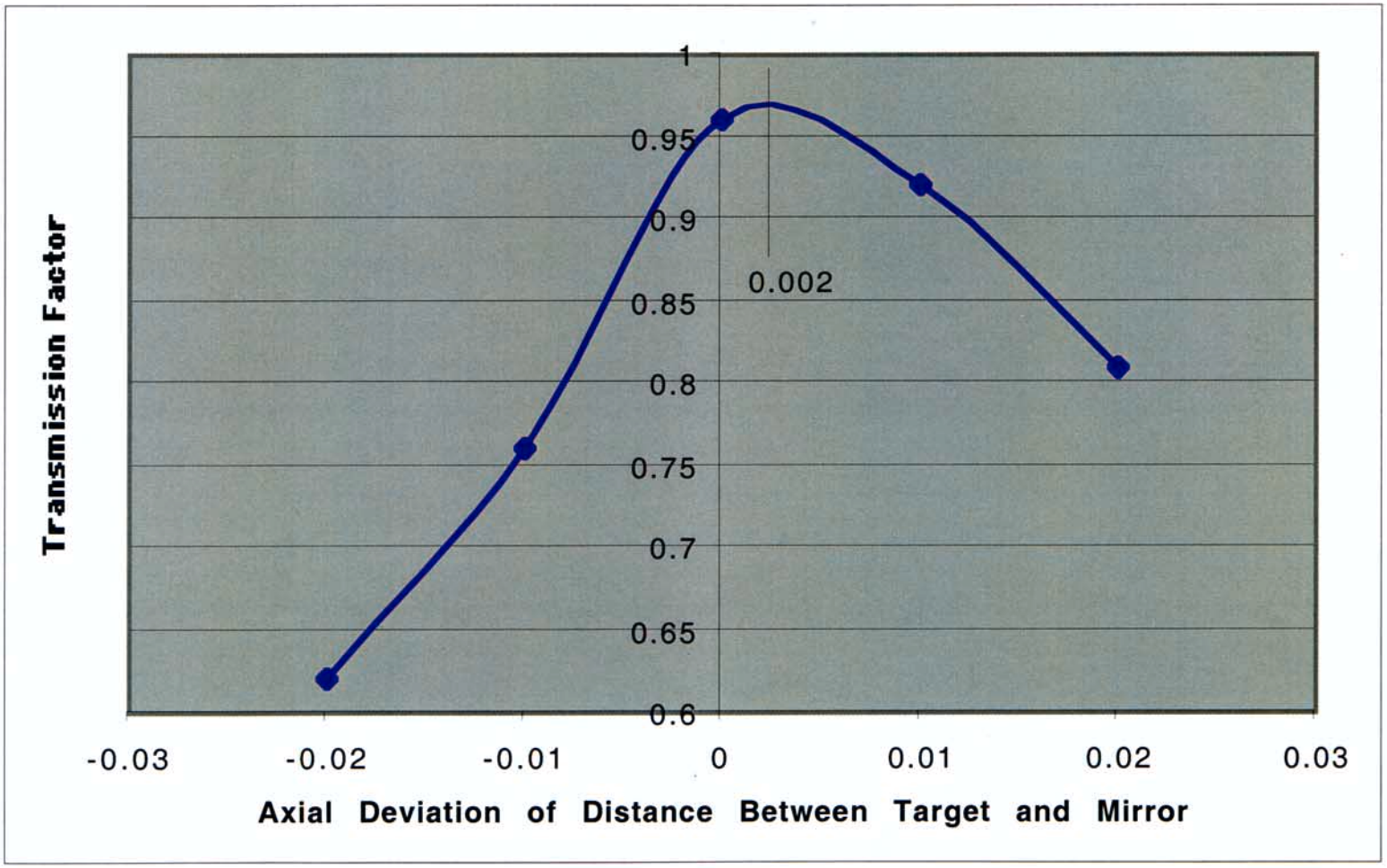

Figure 7(c) Axial Deviation of Distance Between Target and Mirror

FLAT TARGET IMAGE BLUR WITH ELLIPSOID

The same analysis used for the hemisphere is shown for the ellipsoid in Fig. 8. An important difference shown by the ray trace display is that the target image point returns to the source point. Transverse movement of the target has a large tolerance.

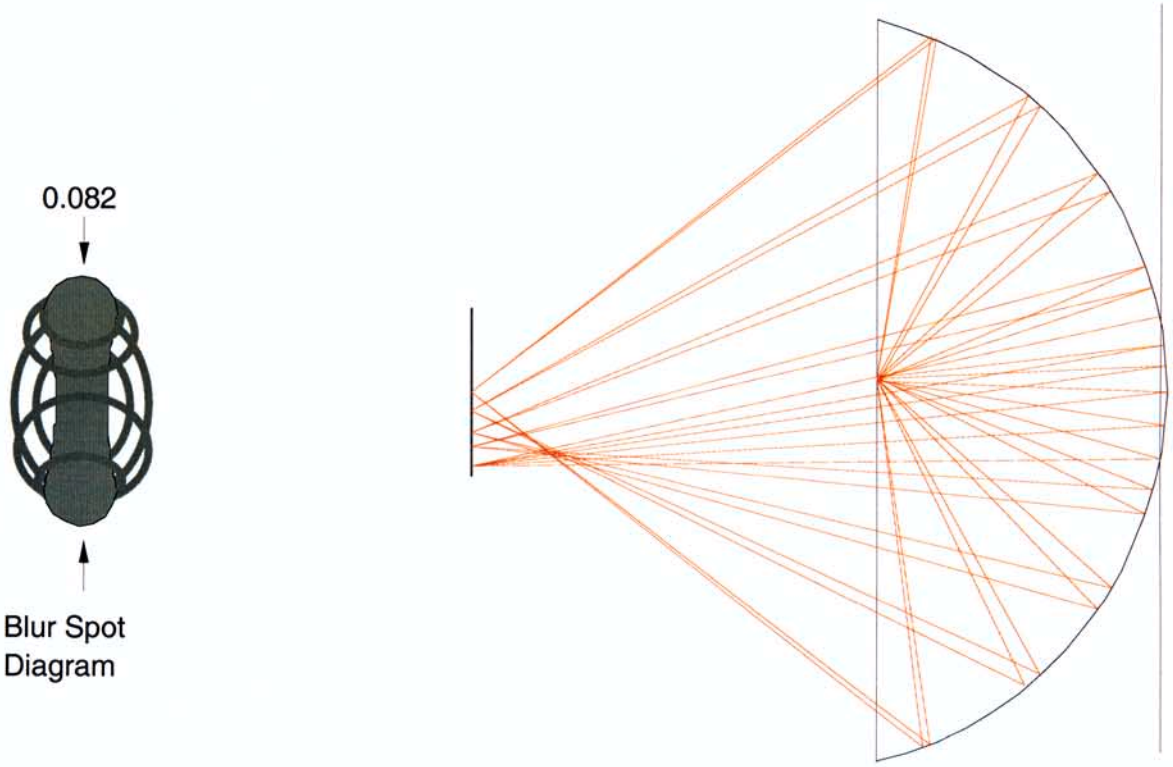

Figure 8(a) Ellipsoid Image Blur; Ray Trace

An intermediate image formed at the lens is very large but it lies within the lens surface. The final image spot has a height twice the hemisphere image spot.

The Zemax program displaced the off-axis image point -0.0025 inches away from the ellipsoid on axis focus. The axial deviation curve shows an optimum position to be away from best focus by -0.006 for a total -0.0085 inch. Adding zero distance contributed by the hemisphere, the optimum target thickness is 0.0085 inch, and its mid-point is 4.004 inch from the hemisphere. The target thickness can be increased on the ellipsoid side by moving the lens surface away from the cavity. For a thickness increase to .032 inch, the lens distance increases by 0.069 inch. For a thickness increase to .062 inch, the lens distance increases by 0.141 inch. In both examples the image edge response curve is improved.

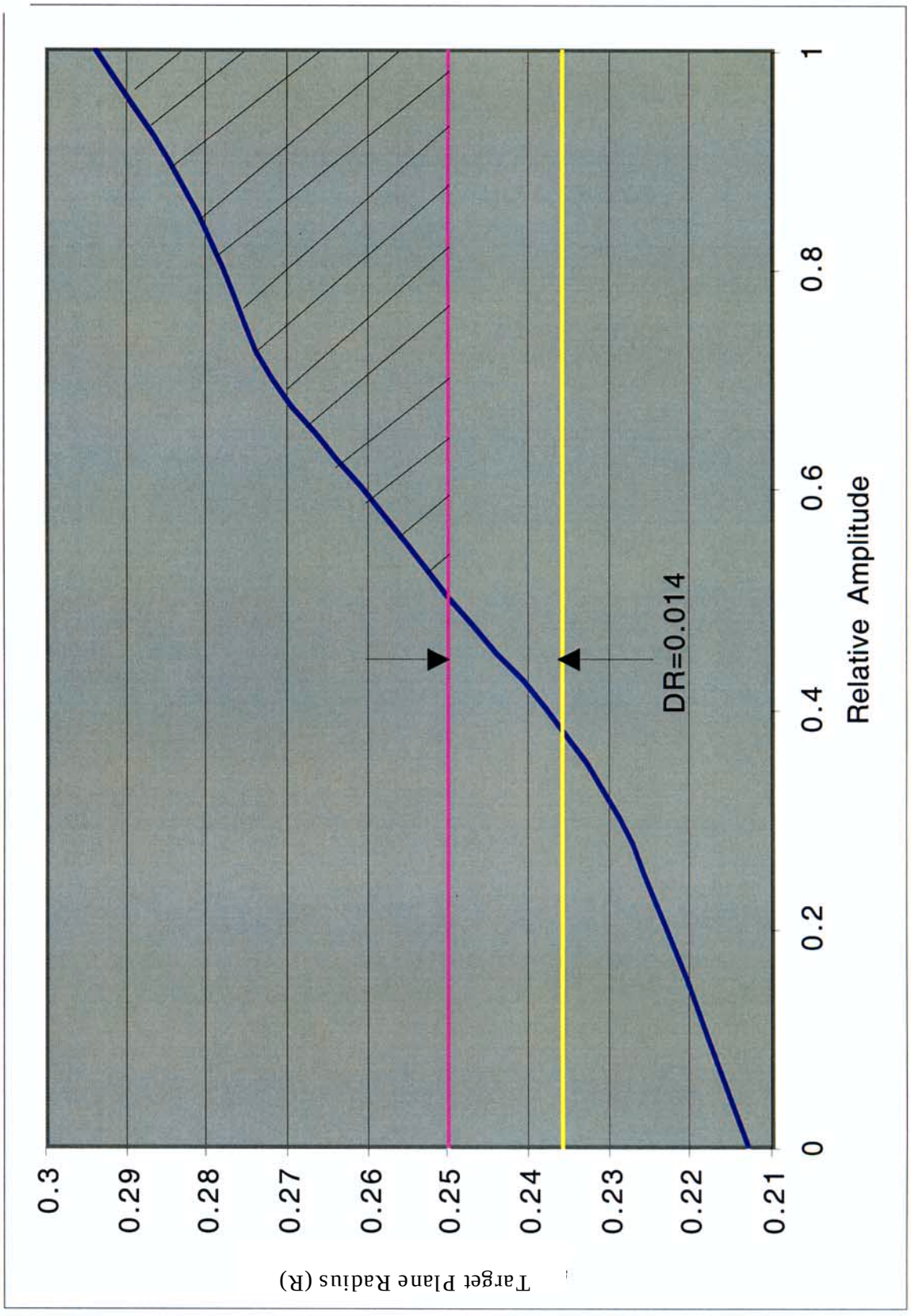

Figure 8(b) Edge Response of Point Image

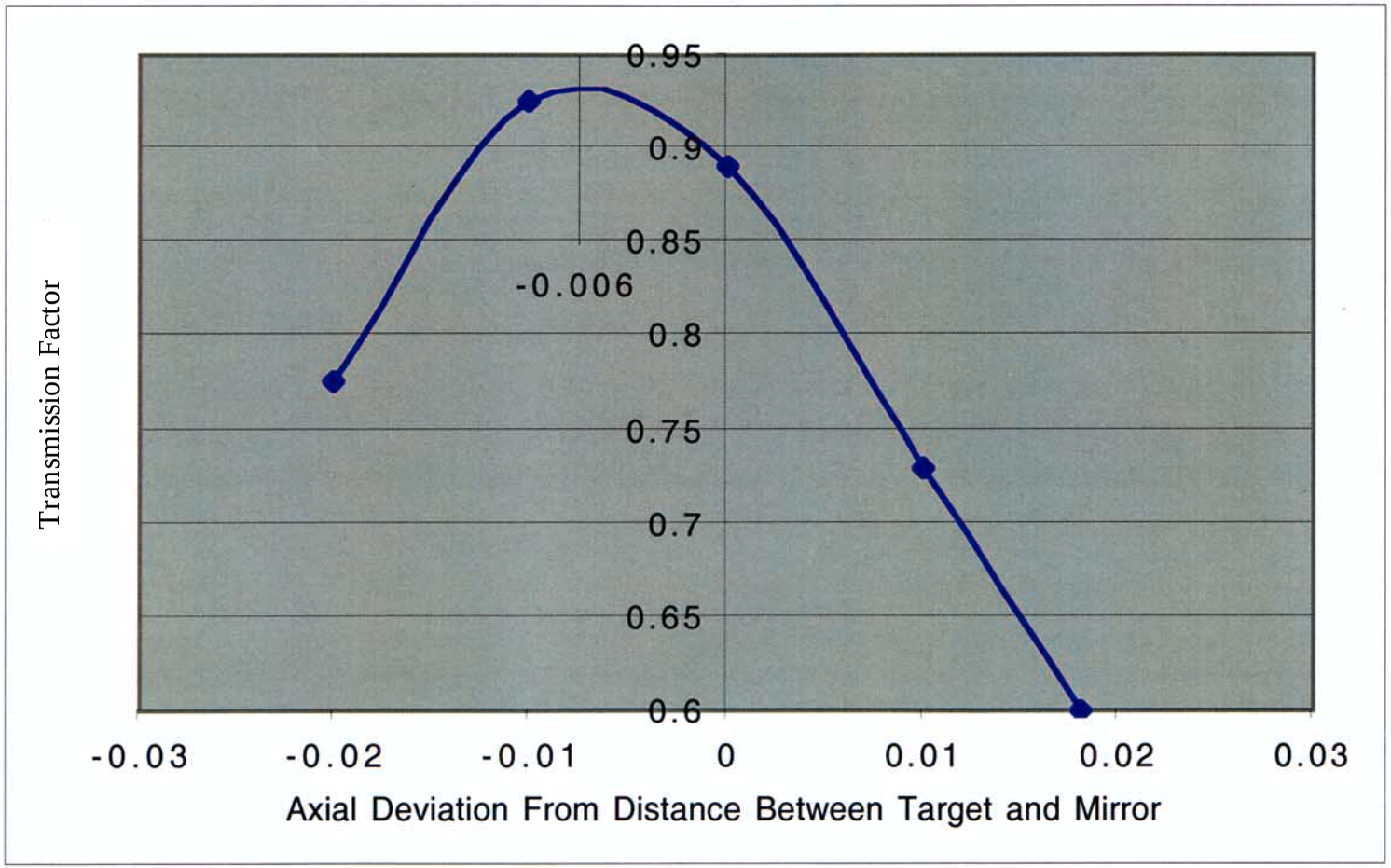

Figure 8(c) Axial Deviation from Distance Between Target and Mirror

At the optimum target position, -0.0085 inch, the transmission factor is τ_E = 0.93. An axial deviation of 0.005 inch from this point has a transmission factor τ_B = 0.90, a reduction of three percent.

The cavity surface ripple causes image blur. For one milliradian slope of the ripple at a 3 inch distance to the target the ray deviation at the target is 0.006 inch. The rms diameter of this blur spot can be combined with the rms diameter of the focus blur spot as an rms of their two diameters in the radial direction.

TEMPERATURE OF FLAT TARGET WITH NO INFRARED REFLECTION LENS COAT

Power Absorbed by Target

The incident power P_0 from the collector in Fig.1(a) is within a cone half-angle 29 degrees and a 1 inch radius image. The image radiance is simplified with an average over its area, and an integrated wavelength spectrum. The power is converted to beam radiance N where $P_0=\pi N(\pi R^2)\sin^2\theta$ giving

$$N = P_0/[\pi(\pi 1^2)\ \sin^2(29\ \text{deg})]\quad \text{watts/in}^2\ \text{steradian} \tag{2}$$

The power focused on a target area by the ellipse subtends a hemisphere. This incident power within an area of radius R less than the maximum 2R=0.567 inch in Fig. 2(a), including transmission and reflection loss with the lens coat $\tau_2(\lambda)$ is

$$P_1 = \tau_1\tau_L\tau_2(\lambda)\tau_P\tau_{P,hE}\rho_M\ [\pi N(\pi R^2)\ \sin^2(90\ \text{deg})]\quad \text{watts} \tag{3}$$

The input power absorbed by the target material is a fraction α. A reflected part $1-\alpha$ goes to the ellipsoid, then focuses to its image at the lens, then reflects to the ellipsoid and is again focused on itself to recover otherwise lost power. The multiple passes accumulate as binomial series $(1 + x + x^2 + x^3 + x^4$ ---) with the sum $[1/(1-x)]$.

The fraction F of power P, Eq. (3), absorbed by the target including an increase by multiple passes is derived in Appendix I, giving

$$F = \alpha\ \{1/[1\ -\ (1-\alpha)\rho_M{}^2\rho_2(\lambda)\tau_P\tau_{P,HE}\tau_E]\} \tag{4}$$

The power absorbed is

$$P_A = P_1F \tag{5}$$

The reflecting surface at the lens may be modified by a low reflectance

coat, or by a hot mirror multilayer coat to reflect infrared at long wavelengths and transmit solar flux at short wavelengths. In this case the fraction of solar power recovered will depend on $\tau_2(\lambda)$ and $\rho_2(\lambda)$ at each wavelength.

Thermal Power Radiated From Target

Thermal power is emitted from each side of a flat target of Fig. 4(b) into a hemisphere solid angle. The spectral power is given by the Planck function for a blackbody at temperature T, and area with radius R inches as

$$P_2 = 37405[\pi(2.54R)^2]/\ \{\lambda^5[\exp(14388/\lambda T)]\} \quad \text{watt} \qquad (6)$$

Integration over wavelengths from 0.3 to 4 microns is does not include some power at longer wavelengths. This power is included by use of the Stefan-Boltzmann integral of the Planck function at all wavelengths

$$P_B = 5.6697E\text{-}12\ [\pi(2.54R)^2]\ T^4 \quad \text{watt} \qquad (7)$$

The power difference P_B-P_2 is added in a computer program at the 4 micron wavelength of Eq.(6).

This power loss is reduced by surface emittance $\varepsilon = \alpha$. Further loss reduction is provided by the target reflectance $(1-\alpha)$, treated as independent of wavelength and temperature. Radiation from the target surface facing the hemisphere is reflected and focused back to another point on itself. Part of this reflected radiation is absorbed by α, the other part $1-\alpha$ is again reflected to the hemisphere and has multiple passes before the reflected power becomes small.

The reduced fraction F_1 of power P_2 emitted to the hemisphere is derived in Appendix II, giving

$$F_1 = \alpha\ \{1 - K\alpha\{1/[1 - K(1 - \alpha)]\}\} \qquad (8)$$

where $K = \rho_M\tau_P\tau_H\tau_C$.

The other side of the target in Figure 4(b) radiates to the ellipsoid, then focuses to its image at the lens, then reflects back to the ellipsoid and is again focused on itself. The image blur transmission factor $\tau_E = 0.87$ and probe interception factors $\tau_{P,HE} = 0.98$ and $\tau_P = 0.99$ are applied. The reflecting surface at the lens may be only a low reflectance coat, or a hot mirror multilayer coat to reflect infrared and transmit solar flux at shorter wavelengths as was described for solar flux. In this case the fraction of power recovered will depend on ρ_2 at each wavelength, which is a more complicated analysis. The reduced fraction F_2 of power P emitted is derived in Appendix II, giving

$$F_2 = \alpha\{1 - K\alpha\{1/[1 - K(1 - \alpha)]\}\} \quad (9)$$

where $K = \rho_M^2 \tau_P \tau_{P,EM} \rho_2(\lambda) \tau_E$.

The total power loss is

$$P_E = P_2F_1 + P_2F_2 \quad (10)$$

A Fortran-22 program was written to find the target temperature T for any value of solar power, target absorption α, and mirror reflection factor ρ_M. Also input is an edge wavelength 2.0 micron and filter reflectance 0.03 to match a silica lens not coated. The target temperature makes the thermally emitted power P_E ,Eq. (10) equal to the absorbed solar power P_A , Eq. (6). Results are plotted in Fig. 9 for target absorption of 0.1 and 0.9.

INCREASED POWER ON FLAT TARGET OF GIVEN TEMPERATURE

With Infrared Reflection Coat on Lens

Some radiation escapes the through the lens in Fig. 4 along the ray path in dashed lines. A hot mirror dielectric multilayer coat on lens surface 3 can strongly reflect the longer wavelengths where the total emitted target power to the ellipsoid is greater than the total absorbed solar power. This increases the power incident on the target.

Equations 2 through 10 are written as functions of wavelength, from .3 to 4 microns in steps of 0.05 micron. The filter spectral curve is a step function known as an edge filter. At the edge wavelength the filter changes from low reflection to a high reflection at longer wavelengths. The filter edge wavelength is then varied to find the greatest increase of target temperature over the value with no filter. The Fortran-22 program finds the target temperature as the edge wavelength is varied. The graph in Fig. 10 shows the temperature gain for a target 0.5-inch diameter vs the filter edge wavelength. Comparison of three values of sun power input and three values of target absorption factor show the edge wavelength 1.4 micron is useful for an absorption factor greater than 0.5. For all absorption factors an average edge wavelength is 1.6 micron. The maximum temperature gain is four percent with the absorption factor 0.9.

In another application the target temperature is fixed, and the excess sun power absorbed is extracted from the target to perform a task. A Fortran-22 program was written with the target temperature input and the excess power as output. Results plotted in fig. 11 show a small power increase with the filter at a target temperature 2700 K or greater.

ALIGNMENT OF TARGET IN CAVITY

Alignment of the target is most direct by an optical path through the lens. Using the ray trace in Fig. 1(b), the target as viewed is about 23 inches from the first lens surface. Transverse position relative to the hemisphere is shown by the reflection of light from

the target edge to its image focused at the opposite edge by the hemisphere. For axial position the image of a bright cross can be focused on the target, and its image reflected from the hemisphere will have maximum contrast at the correct position.

ELLIPSE EQUATIONS

Given the hemisphere reflector radius R = 4 in Fig. 1(b), find the ellipse axes of length A and B. The ellipse equation is

$$x^2/A^2 + y^2/B^2 = 1 \qquad (11)$$

To find the constant A in the figure note that the sum of distances from the object and image to any point on an ellipse is 2A. Using the 45-degree triangle the sum of lengths is

$$(2^{1/2} + 1)\ R = 2A, \text{ or} \qquad (12)$$
$$A = 1.207107\ R$$

The length B in Fig.1 (b) using an isosceles triangle is

$$B^2 = A^2 - R^2/4, \text{ or} \qquad (13)$$

$$B = 1.096841\ R$$

CONCLUDING REMARKS

The present cavity and lens design is for a spherical target that could be either opaque or semitransparent. The performance analysis was made using a flat circular target. A similar analysis would apply to a spherical or hemispherical target. The optimum cavity and lens design can depend on the chosen target shape and size. An optimum flat target may have a different absorption coefficient on the two sides.

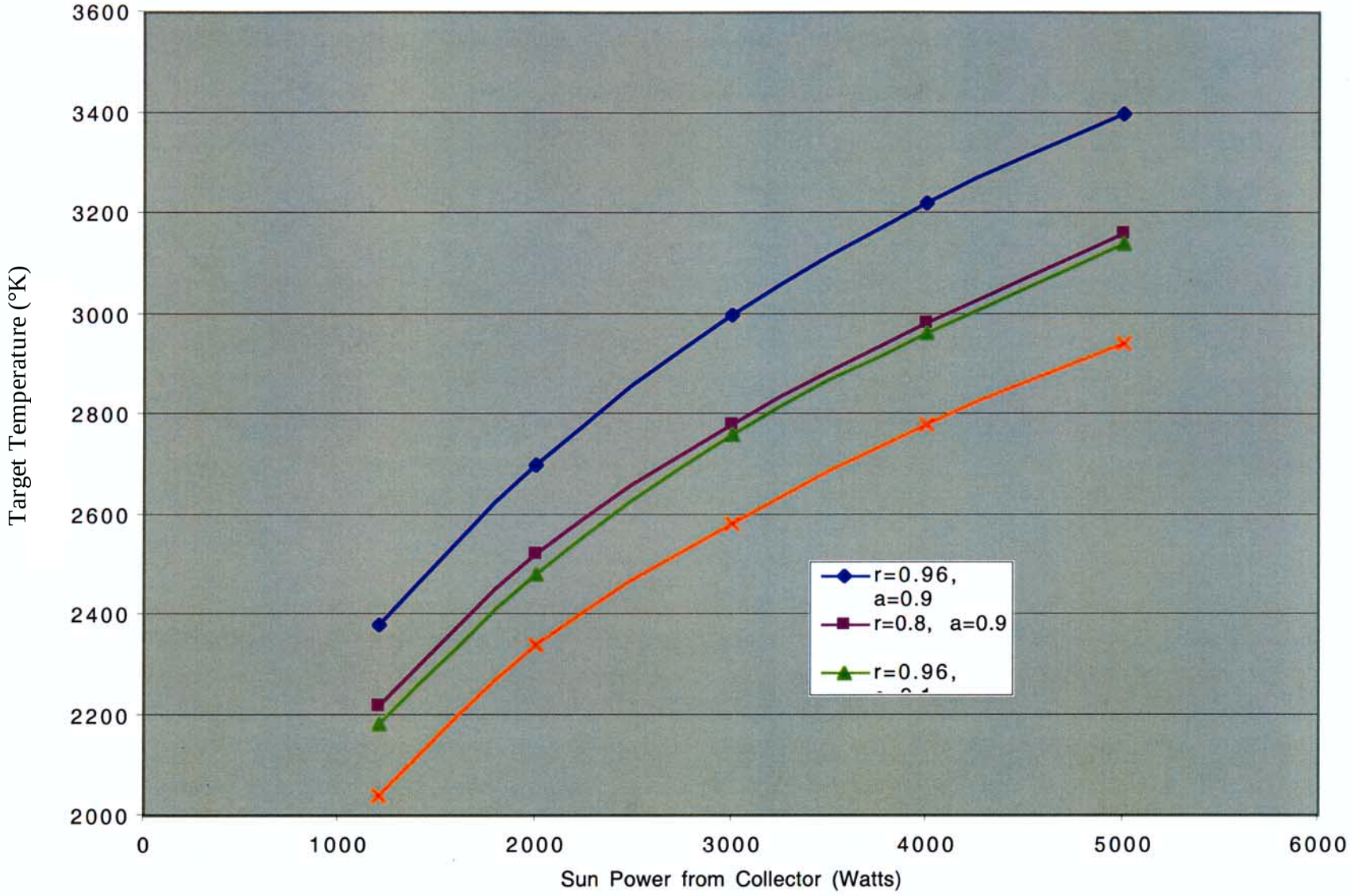

Figure 9 Target Temperature

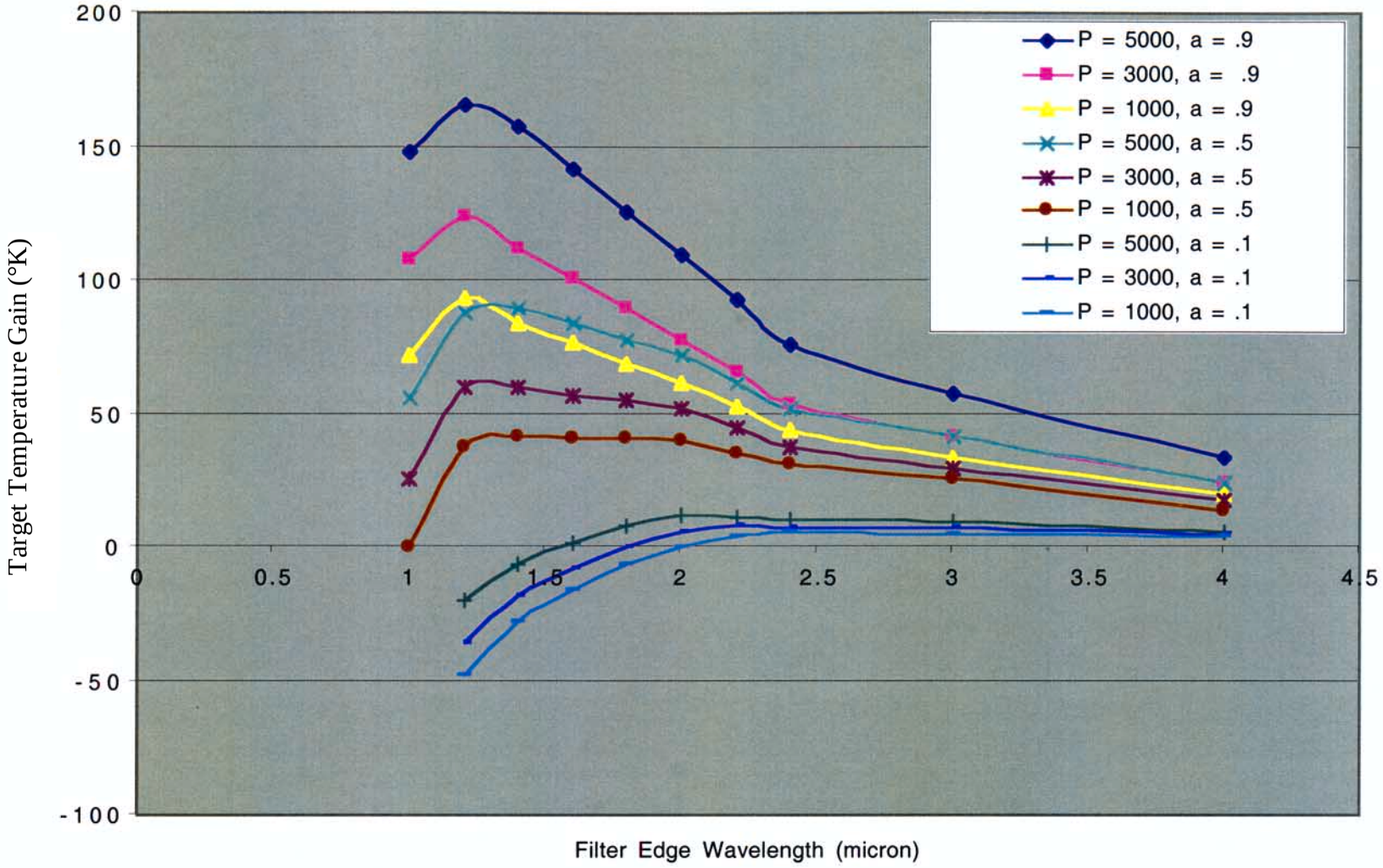

Figure 10 Change in Target Temperature with Addition of EDSE Filter

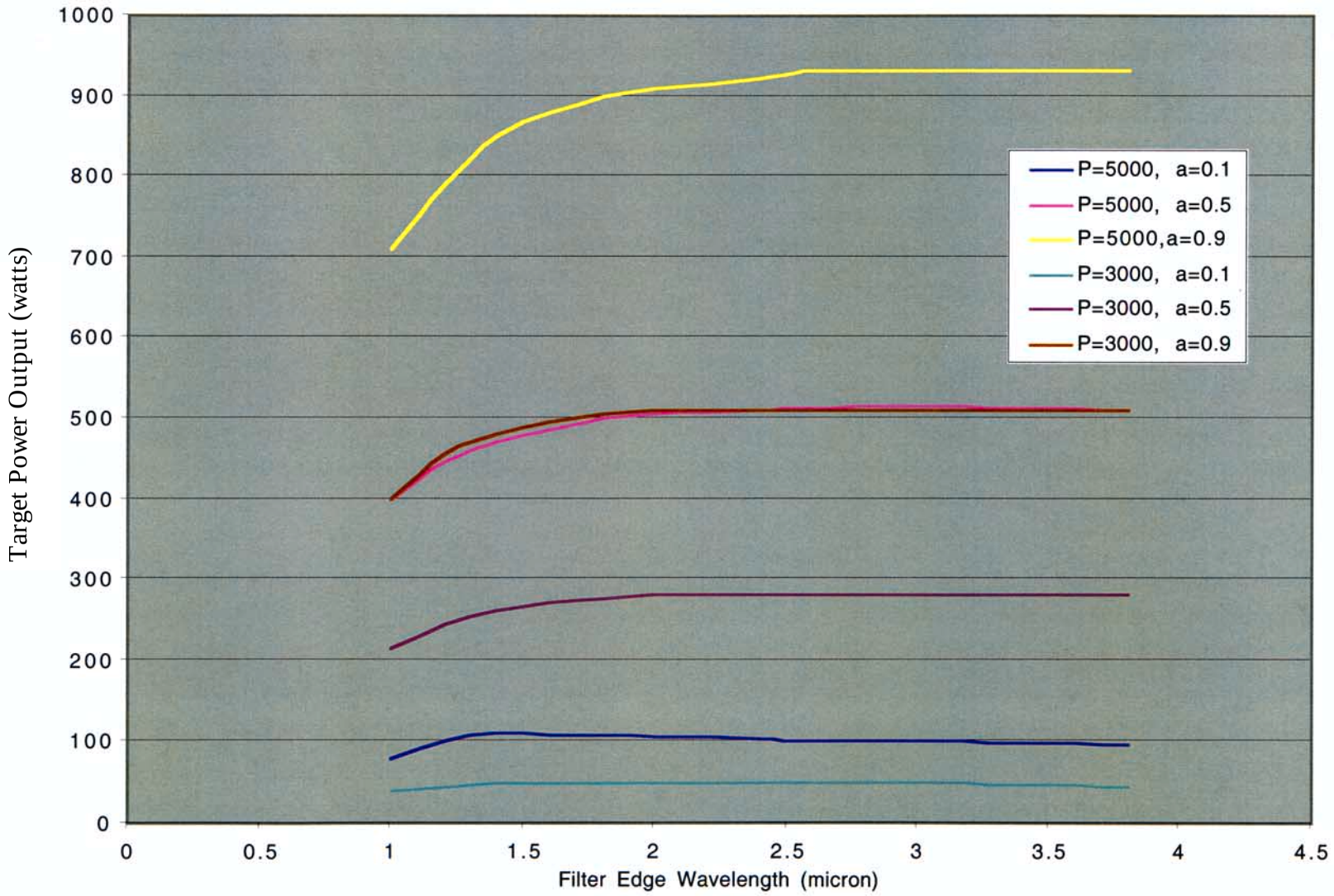

Figure 11(a) Target Power Output at Fixed Target Temperature: Target Temperature 2000°K

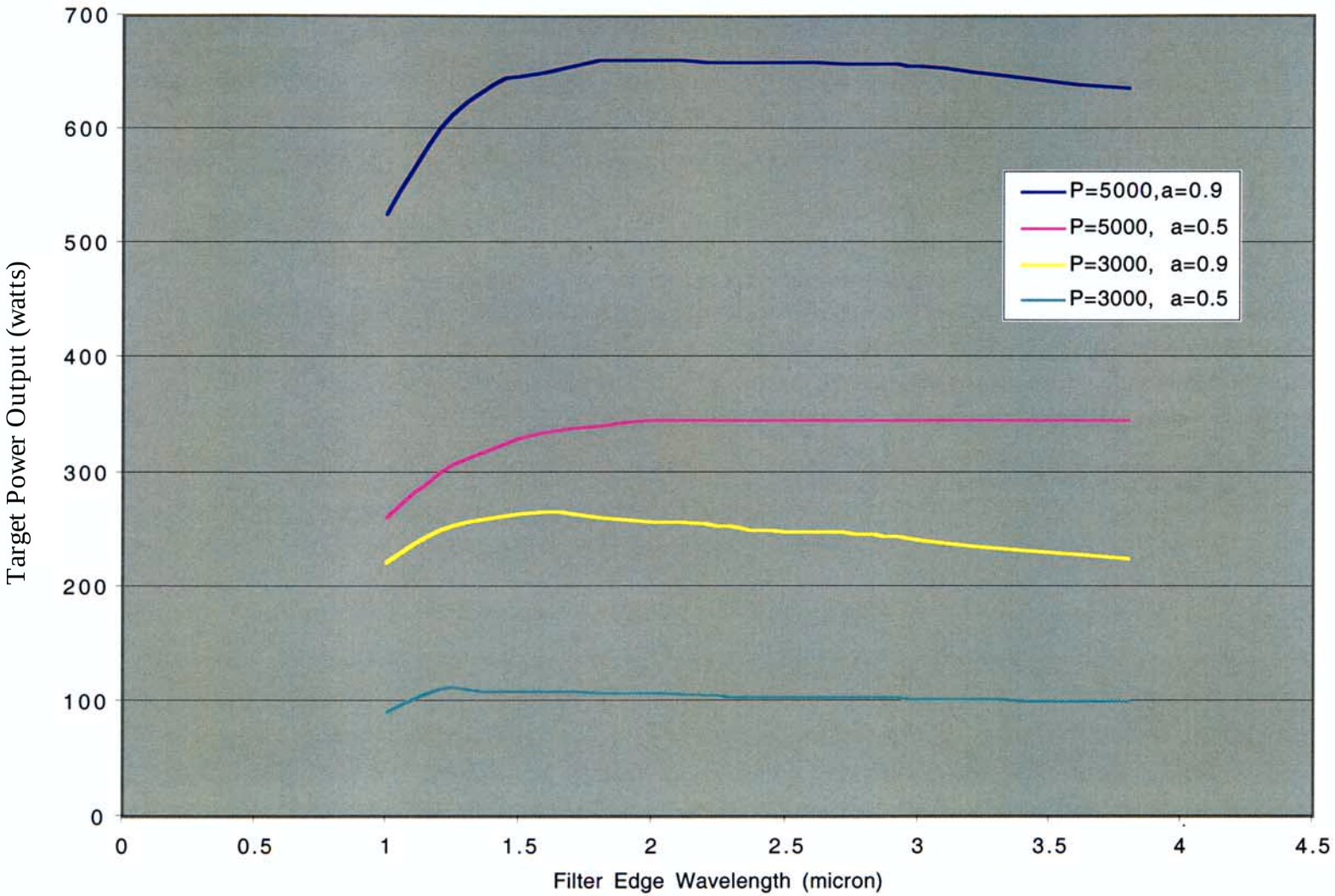

Figure 11(b) Target Power Output at Fixed Target Temperature: Target Temperature 2700°K

APPENDIX I. POWER INTO TARGET

Power incident on a circular target is given by Eq. (3) as P_1. A fraction absorbed by the target is

$$P1=P_1\alpha$$

Incident power P_1 not absorbed is reflected by $1-\alpha$ back to the ellipsoid, past the probe, reflected by the lens, ellipsoid, and then to the target where a fraction α is absorbed, increasing the total power absorbed by

$$P2 = P_1(1-\alpha)K\alpha$$

where transmission along the light path is $K=\rho_M\tau_P\tau_{P,HE}\rho_2\rho_M\tau_E$.

The power P2 not absorbed is also reflected as before, increasing the total absorbed by

$$P3 = P_1(1-\alpha)K(1-\alpha)K\alpha$$

This cycle is repeated until the power added goes to zero. The total power absorbed is

$$P1+P2+P3+P4+ \text{ --- or,}$$

$$\begin{aligned} &P_1\alpha + P_1\,(1-\alpha)K\alpha \\ &\quad + P_1\,(1-\alpha)K(1-\alpha)K\alpha \\ &\quad + P_1\,(1-\alpha)K(1-\alpha)K(1-\alpha)K\alpha \\ &\quad + \text{---} \end{aligned}$$

Combining terms, the total absorbed power is

$$P_1\alpha[1 + (1-\alpha)K + (1-\alpha)^2K^2 + (1-\alpha)^3K^3 + \text{---}]$$

This Binomial series in braces has a solution

$$1/[1-(1-\alpha)K]$$

The fraction of P_1 absorbed by the target is

$$F = \alpha\,\{1/[1-(1-\alpha)K]\}$$

APPENDIX II. THERMAL POWER RADIATION FROM TARGET

Power P_2 emitted from each side of a circular blackbody target at temperature T is given by Eq.(6). The power emitted is reduced by the emittance $\varepsilon = \alpha$ to be

$$P1 = P_2\alpha$$

HEMISPHERE

The emitted power P1 is reflected by the hemisphere mirror to an image point on the circular target, where a fraction α is absorbed to reduce the total radiation loss. The power absorbed is

$$P2 = P_2\alpha\ K\alpha$$

where $K = \rho_M\tau_P\tau_H\tau_C$.

A power fraction $1-\alpha$ is reflected to the hemisphere and back to the target where a fraction α is absorbed. The power absorbed is

$$P3 = [P_2\alpha K(1-\alpha)]\ K\alpha$$

This path is repeated until the power goes to zero. The total power loss is reduced to

$$P1-P2-P3-P4-, \text{ --- or,}$$

$$\begin{aligned} &P_2\alpha - P_2\alpha\ K\alpha \\ &\quad - P_2\alpha\ K(1-\alpha)\ K\alpha \\ &\quad - P_2\alpha\ K(1-\alpha)\ K(1-\alpha)\ K\alpha \\ &\quad - \text{---} \end{aligned}$$

Combining terms the total power loss is

$$P_2\alpha\ \{1-K\alpha[1+K(1-\alpha)+K^2(1-\alpha)^2+ \text{---}]\}$$

The Binomial series term in braces has a solution $1/[1-K(1-\alpha)]$. The fraction F_1 of power P_2 that is a loss is

$$F_1 = \alpha\ \{1-K\alpha\{1/[1-K(1-\alpha)]\}\}$$

Ellipsoid

The power emitted from the target side facing the ellipsoid is given by Eq.(6). The power emitted is reduced by the emittance $\varepsilon = \alpha$ to become

$$P1 = P_2\alpha$$

The emitted power is reflected by the ellipsoid mirror past the probe to the lens surface, reflected back to the ellipsoid, reflected to the target, where a fraction α is absorbed. This increases the total power absorbed by

$$P2 = P_2\alpha\ K\alpha$$

where $K = \rho_M\tau_P\tau_{P,HE}\rho_2\rho_M\tau_E$

The remaining equations are identical to those above giving F_1 for the hemisphere, with a different K.

Reference

1. R. Winston, Editor, "Selected Papers on Nonimaging Optics", SPIE Milestone Series Vol. MS106 (SPIE, Bellingham, Wa., 1995).

2. P.Gleckman,J.O'Gallagher and R.Winston,"Concentration of sunlight to solar-surface levels using non-imaging optics," in Ref. 1, 576-578.

REPORT DOCUMENTATION PAGE

Form Approved
OMB No. 0704-0188

Public reporting burden for this collection of information is estimated to average 1 hour per response, including the time for reviewing instructions, searching existing data sources, gathering and maintaining the data needed, and completing and reviewing the collection of information. Send comments regarding this burden estimate or any other aspect of this collection of information, including suggestions for reducing this burden, to Washington Headquarters Services, Directorate for Information Operations and Reports, 1215 Jefferson Davis Highway, Suite 1204, Arlington, VA 22202-4302, and to the Office of Management and Budget, Paperwork Reduction Project (0704-0188), Washington, DC 20503.

1. AGENCY USE ONLY (*Leave blank*)	2. REPORT DATE	3. REPORT TYPE AND DATES COVERED
	September 2001	Final Contractor Report

4. TITLE AND SUBTITLE

Solar Collector With Image-Forming Mirror Cavity to Irradiate Small Central Volume

5. FUNDING NUMBERS

WU–274–00–00–00
MSFC Grant C–71734–K

6. AUTHOR(S)

Don Buchele, Charles Castle, and Joseph A. Bonometti

7. PERFORMING ORGANIZATION NAME(S) AND ADDRESS(ES)

Northland Scientific Inc.
9970 Brook Road
Olmsted Falls, Ohio 44138

8. PERFORMING ORGANIZATION REPORT NUMBER

E–12911

9. SPONSORING/MONITORING AGENCY NAME(S) AND ADDRESS(ES)

National Aeronautics and Space Administration
Washington, DC 20546–0001

10. SPONSORING/MONITORING AGENCY REPORT NUMBER

NASA CR—2001-211072

11. SUPPLEMENTARY NOTES

Contents were reproduced from the best available copy as provided by the authors. Don Buchele and Charles Castle, Northland Scientific Inc., 9970 Brook Road, Olmsted Falls, Ohio 44138; and Joseph A. Bonometti, University of Alabama, Huntsville, 4701 University Drive, Huntsville, Alabama 35899–0100. Work funded by Marshall Space Flight Center Grant C–71734–K. Project Manager, Dhanireddy R. Reddy, Power and On-Board Propulsion Technology Division, NASA Glenn Research Center, organization code 5430, 216–433–8133.

12a. DISTRIBUTION/AVAILABILITY STATEMENT

Unclassified - Unlimited
Subject Categories: 20 and 74 Distribution: Nonstandard

Available electronically at http://gltrs.grc.nasa.gov/GLTRS

This publication is available from the NASA Center for AeroSpace Information, 301–621–0390.

12b. DISTRIBUTION CODE

13. ABSTRACT ***(Maximum 200 words)***

A unique solar thermal chamber has been designed and fabricated to produce the maximum concentration of solar energy and higher temperature possible. Its primary purpose was for solar plasma propulsion experiments and related material specimen testing above 3000 K. The design not only maximized solar concentration, but also, minimized infrared heat loss. This paper provides the underlying theory and operation of the chamber and initial optical correlation to the actual fabricated hardware. The chamber is placed at the focal point of an existing primary concentrator with a 2.74 m (9 ft) focal length. A quartz lens focuses a small sun image at the inlet hole of the mirrored cavity. The lens focuses two image planes at prescribed positions; the sun at the cavity's entrance hole and the primary concentrator at the junction plane of two surfaces that form the cavity chamber. The back half is an ellipsoid reflector that produces a 1.27 cm diameter final sun image. The image is “suspended in space,” 7.1 cm away from the nearest cavity surface, to minimize thermal and contaminate damage to the mirror surfaces. A hemisphere mirror makes up the front chamber and has its center of curvature at the target image, where rays leaving the target are reflected back upon themselves, minimizing radiation losses.

14. SUBJECT TERMS

Solar; Thermal; Optics; Image-forming; Plasma; Rocket; High-temperature; Reflection; Absorption; Experiment

15. NUMBER OF PAGES

36

16. PRICE CODE

17. SECURITY CLASSIFICATION OF REPORT	18. SECURITY CLASSIFICATION OF THIS PAGE	19. SECURITY CLASSIFICATION OF ABSTRACT	20. LIMITATION OF ABSTRACT
Unclassified	Unclassified	Unclassified	